Renewable Energy 69 (2014) 506–515

Contents lists available at ScienceDirect

Renewable Energy

journal homepage: www.elsevier.com/locate/renene

Assessment of offshore wind energy potential using mesoscale model and geographic information system

Atsushi Yamaguchi [a,*], Takeshi Ishihara [b]

[a] Institute of Engineering Innovation, School of Engineering, The University of Tokyo, 7-3-1 Hongo, Bunkyo, 113-8656 Tokyo, Japan
[b] Department of Civil Engineering, School of Engineering, The University of Tokyo, Japan

ARTICLE INFO

Article history:
Received 13 July 2012
Accepted 10 February 2014
Available online 6 May 2014

Keywords:
Offshore wind energy potential
Mesoscale model
Geographycal information system (GIS)

ABSTRACT

Offshore wind climate along the coast of Kanto area was investigated by a mesoscale model and wind energy potential considering economical and social criteria was estimated by Geographical Information System (GIS). The prediction accuracy of the annual mean wind speed by the mesoscale model was 2.49%. The estimated wind climate shows that offshore Choshi, the annual mean wind speed is significantly higher than other area. Without considering any economical or social criteria, the total potential along the coast of Kanto area is 287 TWh/year, which is slightly more than the annual supply of Tokyo Electric Power Company. If only the bottom mounted foundation is used, the potential varies from 0.21 TWh/year to 7.98 TWh/year depending on the scenario. On the other hand, when floating foundation is taken into consideration, the potential is 100.59 TWh/year even for the most conservative scenario.

1. Introduction

Installed wind energy capacity in Japan is 2,304 MW as of January 2011 [1] and more installation is expected in the future to reduce greenhouse gas emissions. However, the available site for onshore wind farm is now limited. In particular, Tokyo Electric Power Company (TEPCO) has service areas with high demand for electricity while the available site for wind farm is limited. Similar problem exists all over the world and one of the solutions to this problem is to develop a large scale offshore wind farm [2,3]. In Europe, the operation of large-scale offshore wind farm is already started. To increase the wind energy penetration in Japan, the offshore wind development would also be a key issue.

Prior to the large scale offshore development, the assessment of offshore wind energy potential should be investigated. Because the feasibility of offshore wind energy depends not only on the wind climate but also on the economical criteria such as the distance from the coastline, technical criteria such as the water depth or the social criteria such as fishery rights have to be considered and several scenarios shall be compared.

A few study exists for the estimation of offshore wind energy potential around Japan. Nagai and Ushiyama [4] use the measured wind speed at lighthouses and WAsP to estimate the offshore wind energy potential in the area within 3 km from the coastline. Nagai et al. [5] uses the wind speed measurement data at NOWPHAS (Nationwide Ocean Wave information network for Ports and HArbourS) to investigate the probable area for the exploitation of offshore wind energy. These studies, however, use measured wind speed at onshore, with which only near shore potential can be investigated. In practice, the development of offshore wind energy would be difficult in coastal areas due to visual and environmental concerns as is the case in Europe. Thus, the wind energy potential further offshore shall be investigated. Fujii [6] estimated the wind speed above ocean surface using SSM/I image data obtained from DMSP satellite and estimated the wind energy potential over entire Japanese EEZ. This was the first study on quantitative assessment of the total potential offshore wind energy in Japan but the question still remains on the accuracy of the estimation of the wind speed.

In Europe, Garrad et al. [7] estimated the wind climate by combining the wave crest observation and the linear model WAsP [8]. They focused on the area where the water depth is below 40 m and the distance from the coastline is 30 km using Geographical Information System (GIS). The disadvantage of this study is the accuracy of the wind climate assessment by this approach was not verified. Hasager et al. [9] estimated wind speed near ocean surface using remote sensing data of Synthetic Aperture Radar (SAR). They showed that the estimated temporal variation of wind speed shows good agreement with the measurement and investigated the

* Corresponding author. Tel.: +81 3 5841 6217.
E-mail address: atsushi@bridge.t.u-tokyo.ac.jp (A. Yamaguchi).

http://dx.doi.org/10.1016/j.renene.2014.02.024
0960-1481/

special structure of wind speed inside the wake of offshore wind farm. However, the estimation of the absolute wind speed at hub height is still a problem to be solved.

As an estimation method of onshore wind energy potential, wind resource map based on mesoscale model has been widely used [10,11]. However, the accuracy and the applicability of the mesoscale model for offshore wind climate is not yet verified.

In this paper, a method to estimate offshore wind energy using mesoscale meteorological model along the coastline of the Kantô region is proposed and verified by using the measurement data at offshore. Then, quantitative assessment of offshore wind energy potential by using GIS is carried out, considering different scenarios for different social and economical criteria.

2. Prediction and verification of mesoscale weather model

Local wind climate is affected by meteorological phenomena with different scales, from synoptic scale to microscale. The main driving force of the wind is the synoptic scale pressure gradient and both the local circulation and the local topography affect the local wind characteristics. These phenomena can be analyzed by using mesoscale meteorological model, the governing equations of which are the conservation of mass, momentum, heat and water. The boundary and initial conditions are based on the global analysis data. In this study, the mesoscale meteorological model, RAMS (Regional Atmospheric Modeling System) developed at Colorado State University [10] was used to analyze the wind climate along the coastline of Kanto area for year 2000.

2.1. Mesoscale meteorological model RAMS

In RAMS, the conservations of mass, momentum heat and water are solved under initial and boundary condition to obtain three components of wind speed, virtual temperature, exner function and mixing ratio as the function of three dimensional field. The conservations of momentum for x, y and z directions are as follows.

$$\frac{\partial u}{\partial t} = -u\frac{\partial u}{\partial x} - v\frac{\partial u}{\partial y} - w\frac{\partial u}{\partial z} - \theta\frac{\partial \pi'}{\partial x} + fv + \frac{\partial}{\partial x}\left(K_m\frac{\partial u}{\partial x}\right) + \frac{\partial}{\partial y}\left(K_m\frac{\partial u}{\partial y}\right) + \frac{\partial}{\partial z}\left(K_m\frac{\partial u}{\partial z}\right) \quad (1)$$

$$\frac{\partial v}{\partial t} = -u\frac{\partial v}{\partial x} - v\frac{\partial v}{\partial y} - w\frac{\partial v}{\partial z} - \theta\frac{\partial \pi'}{\partial y} - fu + \frac{\partial}{\partial x}\left(K_m\frac{\partial v}{\partial x}\right) + \frac{\partial}{\partial y}\left(K_m\frac{\partial v}{\partial y}\right) + \frac{\partial}{\partial z}\left(K_m\frac{\partial v}{\partial z}\right) \quad (2)$$

$$\frac{\partial w}{\partial t} = -u\frac{\partial w}{\partial x} - v\frac{\partial w}{\partial y} - w\frac{\partial w}{\partial z} - \theta\frac{\partial \pi'}{\partial z} - \frac{g\theta'_v}{\theta_0} + \frac{\partial}{\partial x}\left(K_m\frac{\partial w}{\partial x}\right) + \frac{\partial}{\partial y}\left(K_m\frac{\partial w}{\partial y}\right) + \frac{\partial}{\partial z}\left(K_m\frac{\partial w}{\partial z}\right) \quad (3)$$

The notations used in these equations are summarized in Table 1. The conservation of mass can be written as:

$$\frac{\partial \pi'}{\partial t} = -\frac{R\pi_0}{c_v\rho_0\theta_0}\left(\frac{\partial \rho_0\theta_0 u}{\partial x} + \frac{\partial \rho_0\theta_0 v}{\partial y} + \frac{\partial \rho_0\theta_0 w}{\partial z}\right) \quad (4)$$

In RAMS, ice-liquid water potential temperature proposed by Tripoli and Cotton [11], which is conserved regardless of the phase change of water, is used as an independent variable of the conservation of heat.

Table 1
The definitions of the symbols used in this study.

Symbol	Definition
u	East–West wind component
v	North–South wind component
w	Vertical wind component
f	Coriolis parameter
π	Exner function perturbation term
K_m	Eddy viscosity coefficient for momentum
K_h	Eddy viscosity coefficient for heat and moisture
θ_{il}	Ice-liquid water potential temperature
r_n	Water mixing ratio species of total water, rain, pristine crystals, aggregates, and snow
ρ	Air density
rad	Subscripts denoting tendency from radiation parameterization
g	Gravity
r_t	Total water mixing ratio
r_v	Water vapor mixing ratio
π	Perturbation Exner function
θ_v	Virtual potential temperature

$$\frac{\partial \theta_{il}}{\partial t} = -u\frac{\partial \theta_{il}}{\partial x} - v\frac{\partial \theta_{il}}{\partial y} - w\frac{\partial \theta_{il}}{\partial z} - +\frac{\partial}{\partial x}\left(K_h\frac{\partial \theta_{il}}{\partial x}\right) + \frac{\partial}{\partial y}\left(K_h\frac{\partial \theta_{il}}{\partial y}\right) + \frac{\partial}{\partial z}\left(K_h\frac{\partial \theta_{il}}{\partial z}\right) \quad (5)$$

The conservation of water is shown below.

$$\frac{\partial r_n}{\partial t} = -u\frac{\partial r_n}{\partial x} - v\frac{\partial r_n}{\partial y} - w\frac{\partial r_n}{\partial z} - +\frac{\partial}{\partial x}\left(K_h\frac{\partial r_n}{\partial x}\right) + \frac{\partial}{\partial y}\left(K_h\frac{\partial r_n}{\partial y}\right) + \frac{\partial}{\partial z}\left(K_h\frac{\partial r_n}{\partial z}\right) \quad (6)$$

Other sub models such as radiation model, cumulus model, vegetation model and turbulence model are implemented in RAMS as shown in Table 2. Mellor–Yamada level 2.5 scheme [12] was used for vertical eddy viscosity. The scheme is based on the prognostic equation for the turbulent kinetic energy, which is solved in the meteorological model. The communication between the nested grid and its parent grid is two-way following the technique described by Clark and Farley [13].

At the land and sea surface, the flux of each equation is given according to the method proposed by Louis [14]. At the side and upper boundary, the equations are nudged to the global analysis data.

2.2. Computational settings

In this paper, two level nested grids were used for the wind climate simulation. The outer Grid has 10 km horizontal resolution and covers whole of Kanto region included surrounding mountains, intended to consider the influence of large topography. The offshore area of the interest including the coastline is covered with

Table 2
Physical models in RAMS.

Governing equations	3 Dimensional Boussinesque approximate non-gravitational pressure equation
Horizontal coordinate	Polar stereo graph
Vertical coordinate	σ_z system of coordinates
Vapor precipitation process	Level 2 (including cloud formation)
Turbulence model	Horizontal: Smagorinsky Deformation Vertical: Mellor–Yamada level 2.5 [12]
Atmospheric radiation model	Chen and Cotton [15]
Ground level process	Leaf-2 model [16]

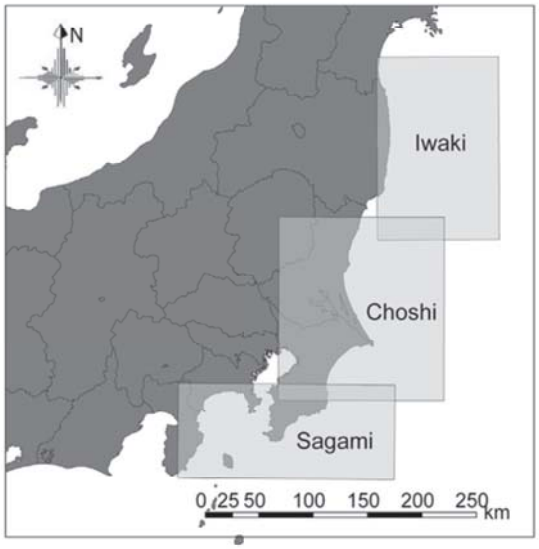

Fig. 1. The inner grids of the each computational domain settings of the mesoscale model.

the inner grid which has 2 km horizontal resolution. In order to cover the coastline of the interest, three different computational domain settings were used, which are named Iwaki, Choshi and Sagami respectively. The inner grids of these settings are shown in Fig. 1 and the details of these domain settings are summarized in Table 3.

The minimum interval of the vertical grid has to be fine enough to represent the vertical wind speed profile and set to 20 m for the inner grid and 40 m for the outer grid. The interval of the vertical grid increases at the higher level and its maximum is 1000 m. The height of the computational domain is set to 25 km.

As the initial and boundary condition, operational atmospheric model archive from European Medium-range Weather Forecast Center (ECMWF) was used. The one year simulation was carried out through the year 2000 in order to estimate the wind climate.

2.3. Verification at Iwaki offshore measurement site

The simulated wind field was verified by using the measured wind speed and direction at Iwaki Offshore Natural Gas Platform, which is located 37 km offshore. The measurement was carried out from October 2004 to September 2006 at 94 m above sea level [17]. Fig. 2 shows the daily average wind speed from December 2004 to November 2005 (one year) and Fig. 3 shows the 10-minute averaged wind speed in June 2005. The solid lines show the simulation while the dashed line shows the measurement. The prediction error of the annual mean wind speed is 2.49%, which means that the 2 km resolution is fine enough for the estimation of offshore wind climate and mesoscale simulation can be used for the wind resource assessment.

The simulated wind direction also shows good agreement with the measurement and shows clear seasonal variation of the prevailing wind direction. Fig. 4 (a) shows the measured and predicted annual wind rose at the Iwaki Offshore Natural Gas Platform. The solid line shows the simulation and the gray shade shows the measurement. The prevailing wind direction of the north-westerly and the southerly can be simulated. Fig. 4 (b), (c) and (d) is the wind roses for February, June and October respectively. During winter, north-westerly winds are observed. When the spring comes, the prevailing wind direction changes to southerly. At the end of the summer, the north-westerly and north-north-westerly winds become more dominant. Those seasonal variations can also be simulated by the mesoscale simulation.

2.4. Spatial distribution of wind along the coastline of Kanto

Wind speed varies due to the surrounding orography and surface roughness, which means the offshore wind climate also vary depending on the location. Fig. 5(a) shows the simulated annual mean wind speed along the coastline of interest. The mean wind speed is generally lower near the coastline and becomes higher as the distance from the coastline increases. It is also noticed that there are significant differences in wind speed depending on location even if the distance from the coast is the same. Fig. 6 shows the distribution of annual mean wind speed along the coastline for different distance from the shore, 0 km, 5 km, 10 km, 20 km, 30 km, and 40 km. For all the cases, the highest annual mean wind speed can be found near Choshi. When the distance from the coastline is small, the annual mean wind speed decreases significantly at the northern coast while it does not when the distance from the coastline is 40 km. At the southern coast, the decrease of the annual mean wind speed is not so significant.

The spatial distribution of mean wind speed depends on seasons. Here, three typical months, February, June and October, are chosen and the monthly mean wind speeds for those three months are shown in Fig. 5(b), (c) and (d) respectively.

In February, when the prevailing wind direction is north-westerly, the mean wind speed near the coast is low and increases considerably as the distance from the coastline increases. This is because the north-westerly wind decreases over obstacles of mainland Japan and increases again over Pacific Ocean.

In June, the prevailing wind direction changes to south–south-westerly and the difference in monthly mean speed is smaller in coastal direction because there are few obstacles for south–south-westerly wind. There exist some areas with slight increase of wind speed at offshore Choshi and Iwaki, which are caused by the low onshore wind speed over Choshi and Iwaki due to strong stratification of atmosphere.

Table 3
The computational domain settings.

Grid		Iwaki	Chôshi	Sagami
Outer grid	Grid center	37°00′ N 140°30′ E	36°00′ N 139°30′ E	35°40′ N 139°30′ E
	Horizontal grid interval	10 km × 10 km	10 km × 10 km	10 km × 10 km
	Number of horizontal grid	55 × 84	77 × 53	54 × 50
	Vertical grid interval	40 m–1000 m	40 m–1000 m	40 m–1000 m
	Number of vertical grid	30	30	30
Inner grid	Grid center	37°20′ N 141°30′ E	36°00′ N 140°45′ E	35°00′ N 140°00′ E
	Horizontal grid interval	2 km × 2 km	2 km × 2 km	2 km × 2 km
	Number of horizontal grid	56 × 84	76 × 84	100 × 44
	Vertical grid interval	20 m–1000 m	20 m–1000 m	20 m–1000 m
	Number of vertical grid	34	34	34

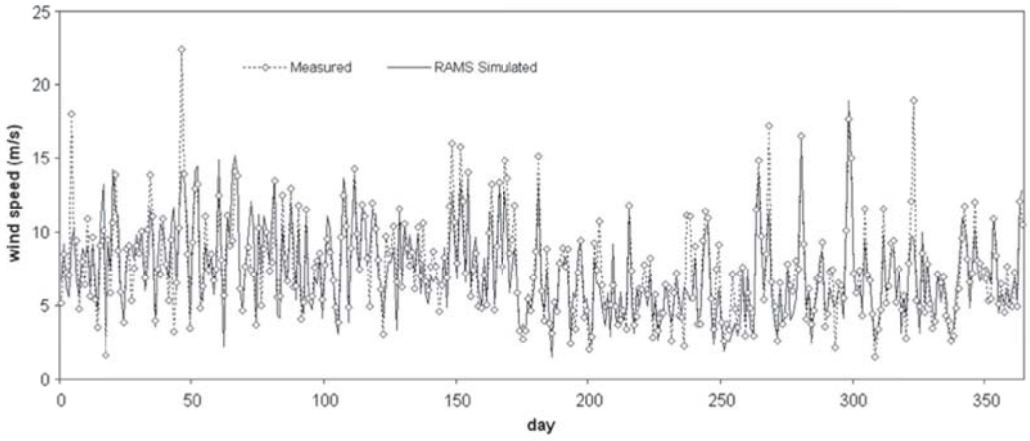

Fig. 2. The daily averaged wind speed from December, 2004 to November, 2005 at the Iwaki measurement site.

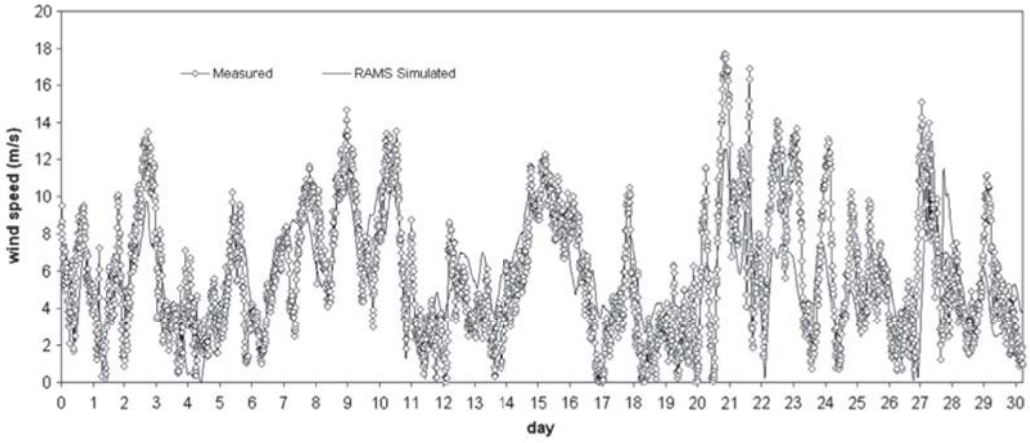

Fig. 3. 10-minute mean wind speed for June 2005 at the Iwaki measurement site.

In October, the prevailing wind direction is north–north-easterly, which means that the wind blows almost parallel to the coastline, resulting in the small difference in wind speed at the coastal area and the offshore area.

3. Evaluation of offshore wind energy

The wind energy potential is the maximum amount of wind energy per year that could be generated based on current technology. In this study, the area 50 km from the coastline in Kanto region excluding Tokyo Bay (see Fig. 7) is considered and the wind energy potential is calculated as a function of water depth and the distance from the coastline. Furthermore, in order to consider the constrained potential and economically competitive potential, several scenarios are proposed and the wind energy potentials are estimated for those scenarios.

3.1. The geographical data

To estimate the wind energy potential for several scenarios, various geographical data are needed. For the estimation of the potential as a function of water depth and the distance from the coastline, isobaths and the coastline data are needed. In order to estimate the wind energy potential for different scenarios, geographical data for National Parks, fishery rights and ports are needed. Table 4 summarizes the geographic data sources used in

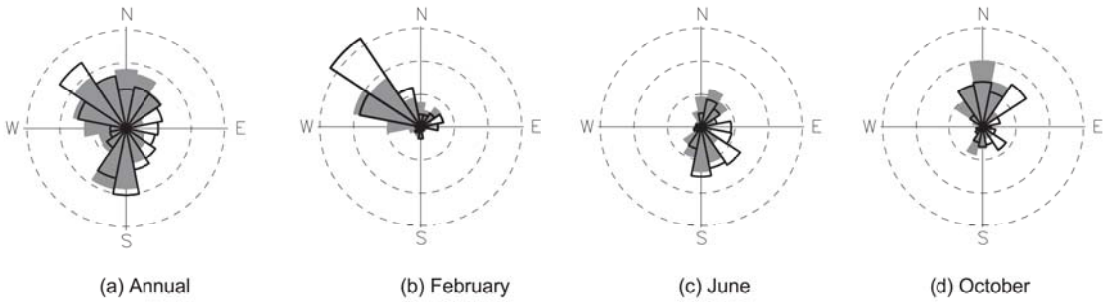

Fig. 4. The wind roses at Iwaki Offshore Natural Gas Platform in the year 2005.

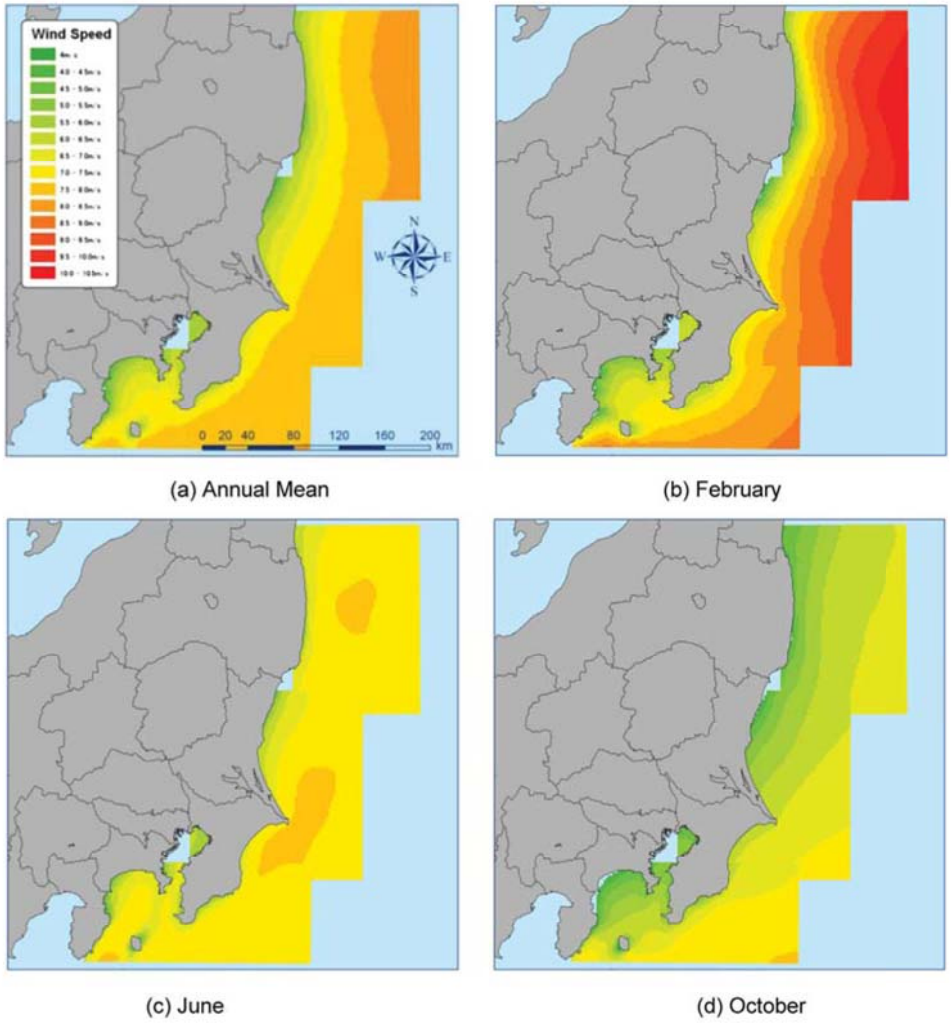

Fig. 5. Mean wind speed along the coast of Kanto Area at 70 m above sea level.

this study. Fig. 8 and Fig. 9 are the example of the data. Fig. 8 shows the water depth and Fig. 9 shows the restricted areas such as fishery rights, national parks and harbor area.

3.2. Wind turbine

For the estimation of the wind energy potential, the power curve of wind turbine has to be assumed. In this study, MWT-92/2.4 [18] by Mitsubishi Heavy Industry was assumed because this class

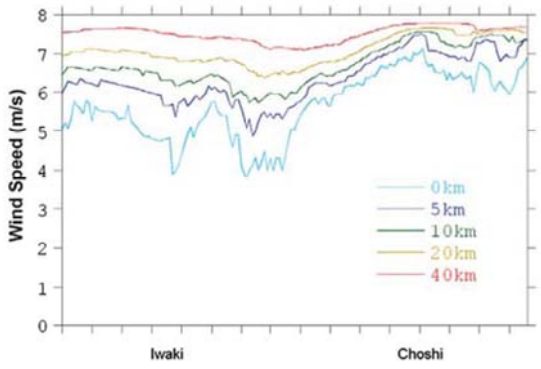

Fig. 6. The annual mean wind speed for different distance from the coastline at 70 m above sea level.

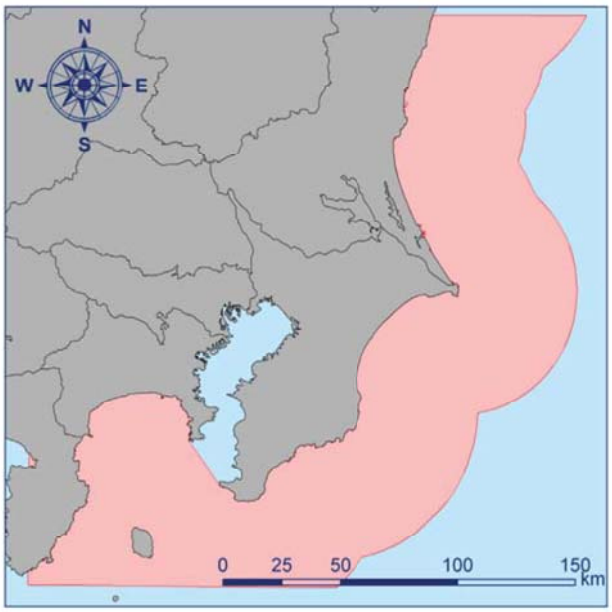

Fig. 7. The domain where the potential wind energy is estimated.

Table 4
The list of the geographical data used in this study.

Geographical data	Dataset	Source
Water depth	Japanese coastal bathymetric data	Marine Information Research Center
Coastline National parks Fishery right Harbor and port	National digitized land information	Ministry of Land, Infrastructure, Transport, and Tourism

of wind turbines is the most commonly used one in large offshore wind farms in Europe. The specification and the power curve of MWT-92/2.4 are shown in Table 5 and Fig. 10 respectively.

The intervals of wind turbines are assumed to be 8 times of the rotor diameter D since the prevailing wind direction in the area of interest varies significantly depending on season as discussed in the previous section. With this interval, the influence of the wake is limited and, thus, the wake effect was not considered in this study.

3.3. Calculation method

The wind energy potential under various scenarios was calculated by superimposing the wind speed calculated by using the mesoscale model and the geographical data on ArcInfo GIS tool. The wind speed at the hub height, which is 70 m above sea level, was linearly interpolated from two adjacent grid points at 52 m and 72 m.

Fig. 11 shows the example of the superimposition of the grid wind speed data and the geographical data. The wind speed is defined for each grid volume with the interval of 2 km by 2 km, as a spatially averaged value over it. Each grid volume is assigned with index numbers along north–south and east–west directions. As shown in Fig. 11, the index i denotes the east–west direction while the index j denotes the north–south direction. The 10-minutes mean wind speed is assumed to be homogeneous across the grid volume.

The power produced by a wind turbine installed in a grid volume with the index (i,j) per year $\mathrm{AEP}_{i,j}$ can be calculated by equation (7):

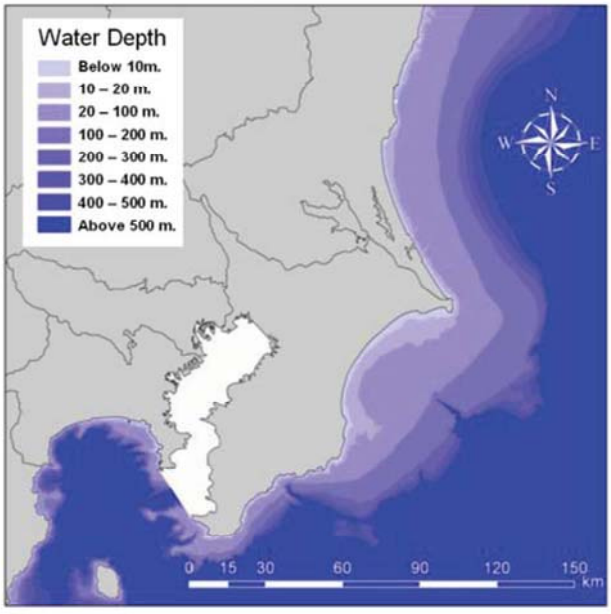

Fig. 8. The water depth across the domain area.

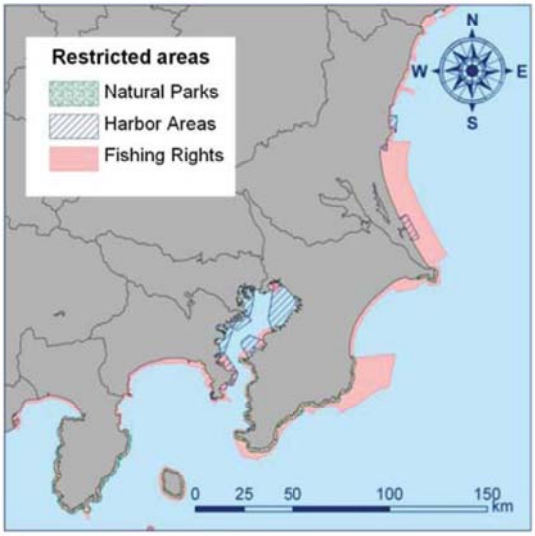

Fig. 9. The prohibited areas across the domain area.

$$\mathrm{AEP}_{i,j} = \sum_{t=1}^{T} P\left(V_n^{i,j,t}\right), \tag{7}$$

where, T is the number of hours per year, which is equal to 8784 in this study as the year 2000 is an intercalary year.

$V_n^{i,j,t}$ is the normalized wind speed considering the effect of the change of air density and calculated by equation (8) according to IEC61400-12 [19]:

$$V_n^{i,j,t} = V_{10\ \mathrm{min}}^{i,j,t}\left(\frac{\rho_{10\ \mathrm{min}}^{i,j,t}}{\rho_0}\right)^{1/3} \tag{8}$$

where, $V_{10\ \mathrm{min}}^{i,j,t}$ is the 10-minutes mean wind speed, calculated by using mesoscale model, ρ_0 is the standard air density at the temperature of 288.15 K and the atmospheric pressure of 101.325 kPa, and $\rho_{10\mathrm{min}}^{i,j,t}$ is the 10-minute averaged air density which is a function of 10-minute mean pressure $p_{10\ \mathrm{min}}$ and temperature $T_{10\ \mathrm{min}}$ (9):

$$\rho_{10\ \mathrm{min}} = \frac{p_{10\ \mathrm{min}}}{R \times T_{10\ \mathrm{min}}} \tag{9}$$

where, R is the gas constant.

The number of wind turbines which can be placed within the grid can be estimated by using equation (10).

$$N_{i,j} = \frac{A_{i,j}}{8D \times 8D} \tag{10}$$

where, A_{ij} is the area suitable for wind energy exploitation in the grid with index i and j (Fig.11). Then, the total amount of energy

Table 5
The specification of the wind turbine used for the estimation of the wind energy potential.

Rotor diameter (D)	92 m
Hub height	70 m
Rated power	2.4 MW
Control	Pitch control
Cut-in wind speed	3 m/s
Cut-out wind speed	25 m/s
Wind turbine intervals	$8D \times 8D$

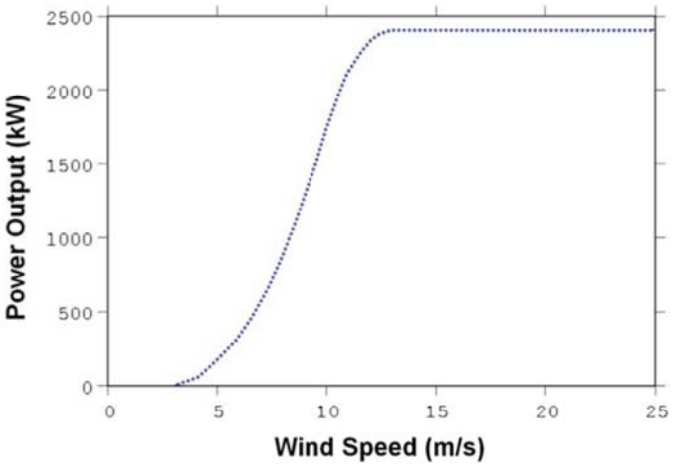

Fig. 10. The power curve of the 2.4 MW wind turbine used for the estimation of wind energy potential.

generated per year in an area can be calculated by using equation (11).

$$\mathrm{AEP}_{\mathrm{total}} = \sum_{i,j} N_{i,j} \times \mathrm{AEP}_{i,j} \tag{11}$$

3.4. Wind energy potential based on distance from coastline and water depth

Using the proposed method, the raw wind energy potential along Kanto coastal region within 50 km from the coastline was calculated for different distance from the coastline and the water depth as shown in Table 6 and Fig. 12. The total offshore potential in this region is estimated to be 286.54 TWh/year, which is more than the annual power production of Tokyo Electric Power Company (TEPCO) which is 280.2 TWh/year in 2010 [20]. However, considerable amount of the potential is situated in the area where water depth is more than 500 m as shown in Fig. 12, which is difficult to exploit due to technical reasons. On the other hand, although the potential of 4.87 TWh/year exists in the area where water depth is less than 10 m, fishery rights are registered in most of this area. This is an example of social constraints. In the next section, the wind energy potential considering the technical, social and economical constraints are estimated assuming some scenarios for each constraint.

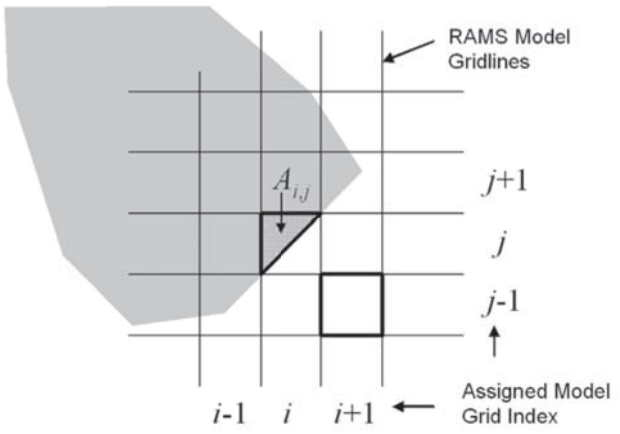

Fig. 11. Overlaying of the geographical data and the results of the mesoscale model.

Table 6
Wind energy potential considering the water depth and the distance from the coastline in TWh/year.

		Distance from coastline (km)					Total
		0–10	10–20	20–-30	30–40	40–50	
Water depth (m)	0–10	4.77	0.00	0.05	0.05	0.00	4.87
	10–20	9.00	0.44	0.05	0.03	0.00	9.51
	20–100	22.49	24.55	5.92	0.42	0.00	53.38
	100–200	4.96	8.56	23.73	9.29	0.26	46.81
	200–300	2.23	1.24	5.28	6.60	0.82	16.18
	300–400	2.16	1.27	3.30	6.38	2.51	15.62
	400–500	1.75	2.61	1.69	5.89	3.58	15.53
	Over 500	5.95	24.26	21.89	29.05	43.50	124.65
Total		**53.31**	**62.93**	**61.92**	**57.70**	**50.68**	**286.54**

3.5. Potential energy considering social and economic constraints

In this section, wind energy potential was calculated considering the social and economic constraints under several scenarios.

Water depth is the primary concern to determine the type of foundation. In Europe, bottom-mounted foundations have been widely used for the area where water depth is less than 20 m. For deeper water, floating foundations have to be used. Even with the floating foundation, the area where the water depth is deeper than 200 m is difficult to use due to economical reason. In this study, two scenarios were considered, in the first scenario, considering the bottom mounted foundation and the use of area where the water depth is less than 20 m is assumed and in the second scenario, both the bottom mounted and floating foundation are considered and the use of area where the water depth is up to 200 m is assumed.

Social constraints such as fishery rights, national parks and environmental concern are also an important criterion. In this study, three scenarios are considered regarding the social constraints. The first scenario does not consider any social constraints, and the second scenarios exclude the area with fishery rights, national parks and ports. Due to visual and environmental concern, the construction of the wind farms close to the shore is limited in Europe. Thus, the third scenario excludes the area within 10 km from the coastline in addition to the excluded areas in the second scenario.

Economical feasibility is also an important criterion. Capacity factor (CF) is often used as an index to evaluate the economical feasibility of wind farm and defined as the ratio of the actual output of the wind farm over certain period of time and its potential output if it had operated at full nominal capacity throughout the entire time.

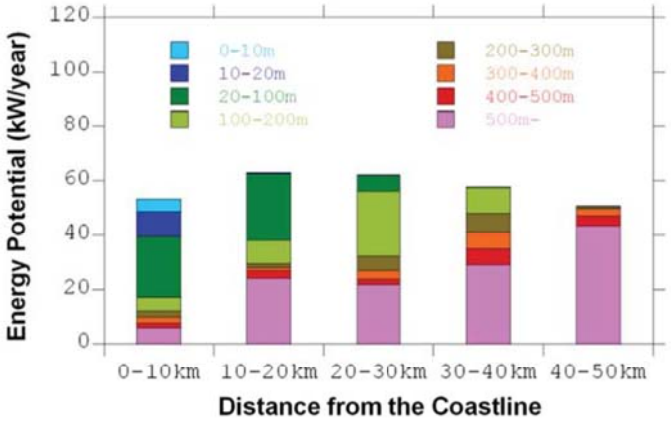

Fig. 12. Wind energy potential considering the water depth and the distance from the coastline.

Table 7
Wind energy potential for each scenario considering the social and economical criteria.

Scenario	Foundation type	Social restriction	Capacity factor	Available area (km^2)	Number of wind turbines	Installed capacity (MW)	Potential (TWh/year)	Relative potential[c] (%)
B0-25	Bottom-mounted and floating	None	>25%	901	1663	3990	11.51	4.11
B0-30			>30%	590	1088	2610	7.98	2.85
B0-35			>35%	125	232	560	1.84	0.66
B1-25		[a]	>25%	354	654	1570	4.71	1.68
B1-30			>30%	292	540	1300	3.98	1.42
B1-35			>35%	79	146	350	1.16	0.41
B2-25		[b]	>25%	15	27	60	0.21	0.07
B2-30			>30%	15	27	60	0.21	0.07
B2-35			>35%	15	27	60	0.21	0.07
F0-25	Floating	None	>25%	10,481	19,345	46,430	150.42	53.68
F0-30			>30%	8977	16,573	39,780	133.42	47.62
F0-35			>35%	5983	11,044	26,510	93.53	33.38
F1-25		[a]	>25%	8837	16,314	39,150	129.14	46.09
F1-30			>30%	7906	14,594	35,030	118.55	42.31
F1-35			>35%	5598	10,334	24,800	87.76	31.32
F2-25		[b]	>25%	7234	13,355	32,050	107.56	38.39
F2-30			>30%	6622	12,225	29,340	100.59	35.90
F2-35			>35%	5106	9427	22,620	80.40	28.69

[a] Excluding the areas with fishing rights, natural park regulations, and port and harbor operations.
[b] Excluding the sea area within 10 km offset distance from the coastline and areas with fishing rights, natural park regulations, and port and harbor operations.
[c] The ratio of wind energy potential over annual energy production of TEPCO in 2009 (280.2 TWh/year).

In this study, the capacity factor was estimated from the time series of wind speed for one year as shown in equation (12).

$$\mathrm{CF} = \frac{E_{\mathrm{A}}(\mathrm{kWh/year})}{P_{\mathrm{rate}}(\mathrm{kW}) \times T(\mathrm{h/year})} \tag{12}$$

For onshore wind farms, if the capacity factor exceeds 20%, the wind farm is said to be economically feasible. In case of offshore wind farm, the construction and maintenance costs would be higher than the onshore wind farm and in this study, as the criterion of the capacity factor, 25%, 30% and 35% are considered as basis of economic scenarios.

A total of 18 scenarios were investigated as a combination of technological, social, and economic factors. Table 7 summarizes each scenario and corresponding potential together with the available area, the number of wind turbines, the possible installed capacity and the potential relative to the annual power production by TEPCO in 2009. The corresponding area where the wind turbine can be installed for each scenarios is shown in Fig. 13.

If only bottom-mounted foundation is considered, the available offshore wind energy potential strongly influenced by social constraints. For example, when the minimum capacity factor is 30% without considering any social constraints (scenario B0-30, Fig. 13(a)), 1088 wind turbines can be installed in 590 km^2. In this

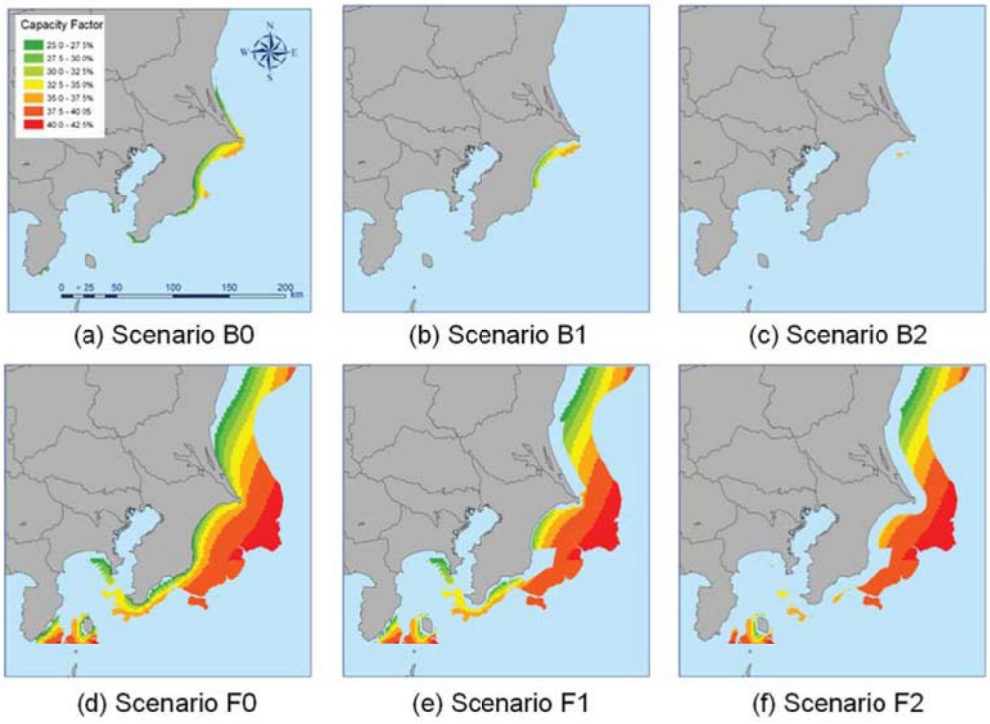

Fig. 13. Spatial distribution of wind energy potential for each scenario.

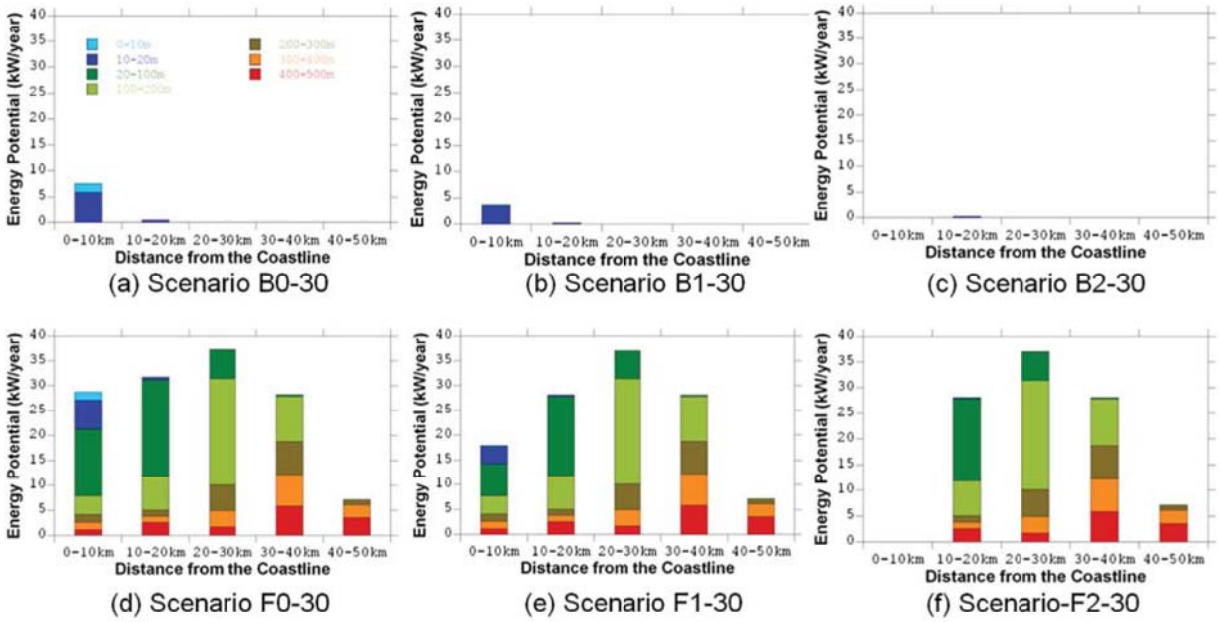

Fig. 14. The wind energy potential for each scenario with the minimum capability factor of 30 percent considering the water depth and the distance from the coastline.

case, the installed capacity would be 2610 MW with potential wind energy of 7.98 TWh/year which is equivalent to 2.85% of the annual power production of TEPCO in 2009. In contrast, when areas with fishery rights, national parks, and harbor areas are excluded (scenario B1-30 and Fig. 13(b)), the available offshore area was decreased to 292 km^2 resulting to 3.98 TWh/year potential energy. Furthermore, if construction of offshore wind farm is prohibited within 10 km from the coastline in addition (scenario B2-30 and Fig. 13(c)), the available sea area becomes 15 km^2 in which only 27 wind turbines can be installed. This scenario yields only 0.21 TWh/year of potential energy, which is equivalent to 0.07% of the annual energy production of TEPCO in 2009. This is because most of the sea areas with the water depth of less than 20 m are located within 10 km from the coastline. This is clear from Fig. 14(a) (b) and (c) which shows the potential of each scenario with the capacity factor more than 30% for different water depth and the distance from the coastline.

The potential increases significantly when floating foundations can be used. In the case that the capacity factor is 30% or more, even when the most severe social restrictions is considered (Scenario F2-30, Fig. 14(f)), 12,225 wind turbines can be installed in the area of 6622 km^2 with a total installed capacity of 29,340 MW. The potential would be 100.59 TWh/year which accounts for 35.9% of the annual energy production by TEPCO in 2009. From Fig. 13(f), it is clear that the available area is distributed far offshore compared to the case in which only the bottom-mounted foundation are used. If no social constraints are considered (Scenario F0-30, Fig. 14(d)), 16,573 wind turbines can be installed in the area of 8977 km^2, resulting in the installed capacity of 39,780 MW. In this case, the potential would be 133.42 TWh/year which accounts for 47.6% of annual energy production by TEPCO in 2009. If port areas, national parks and the areas with fishery rights are excluded (Scenario F1-30 and Fig. 13(e)), the available area would be 7,906 km^2 in which 14,594 wind turbines can be installed resulting in the potential of 118.55 TWh/year, which is equivalent to 42.3% of annual energy production by TEPCO in 2009.

For the scenarios with floating foundation and the capacity factors are more than 30%, the potential is shown for different water depth and the distance from the coastline in Fig. 14 (d) (e) and (f). The scenario with the most severe social constraint, F2-30, has the potential of 100.59 TWh/year, which is equivalent to 35.9% of annual energy production by TEPCO in 2009, in the area with the water depth between 20 m and 200 m and the distance from the coastline between 10 km and 30 km, which should be the target for the future development of the floating offshore wind turbine.

4. Conclusions

In this study, the offshore wind energy potential along the coastline of Kanto region is investigated by using mesoscale model and GIS considering technological, social, and economic constraints. This method is shown to accurately estimate the wind energy potential. Following results were obtained.

- Mesoscale model is accurate enough to estimate the offshore wind energy potential at the site 40 km offshore. The prediction error of annual mean wind speed at Iwaki Natural Gas Platform was only 2.49%.
- Spatial distribution of wind speed and the prevailing wind direction along the coastal area of Kanto region significantly depend on season. In winter, the prevailing wind direction is north-westerly and the wind speed rapidly increases as the distance from the coastline increases. In summer, the prevailing wind direction is south-westerly and the wind speed is independent on the distance from the coastline since the wind blows almost parallel to the coastline. Slight increase in the wind speed can be observed at the tip of Choshi Peninsula, where the wind is concentrated. Overall, the wind speed varies depending on the location and relatively high near the tip of Choshi Peninsula.
- When all the sea area within 50 km from the coastline can be used for the exploitation of wind energy, the annual potential of the offshore wind energy would be 287 TWh/year which is slightly more than the annual energy production of TEPCO in 2009.
- If only bottom-mounted foundation can be used, the available area for offshore wind energy is considerably limited. Even if no social restriction is applied, the potential is 7.98 TWh/year for the case that capacity factor is more than 30%, and if the most

conservative restriction is adopted, the potential decreases to 0.21 TWh/year.

- If floating foundation can be used, the potential increases significantly. For the area with minimum capacity with 30%, the potential reaches 100.59 TWh/year even for the most conservative social restrictions. When the distance from coastline is between 10 km and 30 km and the water depth between 20 m and 200 m, the potential will be 39.32 TWh/year, which accounts for 15% of annual energy production TEPCO in 2009. This implies that those areas should be targeted for the future development of the floating offshore wind turbine.

References

[1] Operating wind power capacity. Wind Power Mon 2011;27(1):66.
[2] Gaudiosi G. Offshore wind energy in the world context. In: Proc. World Renewable Energy Conference; 1996. pp. 899–904.
[3] European Wind ENERGY Association and Greenpeace. Wind energy. 12; 2004.
[4] Nagai H, Ushiyama I. Potential of offshore wind power generation in main shorelines of Japan. In: Proc. of JSES/JWEA Joint Conference; 2000. pp. 219–21 [in Japanese].
[5] Nagai T, Katsuumi T, Okajima N, Sumida K, Kudaka M. Potential of wind power around Japanese coastal areas utilizing NOWPHAS system data. Proc Civ Eng Ocean 2001;17:19–24 [in Japanese].
[6] Fujii T. An estimation of the potential of offshore wind power in Japan by satellite data. In: Proc. of JSES/JWEA Joint Conference; 1999. pp. 447–50 [in Japanese].
[7] Garrad AD, Adams BM, Matthies H, Scherweit M, Siebers T. An assessment of the offshore wind potential in the EC. In: Proc. 15th British Wind Energy Conference; 1993. pp. 401–6.
[8] Mortensen NG, Troen I, Landberg L, Petersen EL. Wind atlas analysis and application program (WAsP). Denmark: Risø National Laboratory; 1993.
[9] Hasager CB, Barthelmie RJ, Christiansen MB, Nielsen M, Pryor SC. Quantifying offshore wind resources from satellite wind maps: study area the North Sea. In: Scientific Proceedings of European Wind Energy Conference; 2004. pp. 29–32.
[10] Pielke RA, Cotton WR, Walko RL, Tremback CJ, Lyons WA, Grasso LD, et al. A comprehensive meteorological modeling system – RAMS. Meteorol Atmos Phys 1992;49:69–91.
[11] Tripoli J, Cotton WR. The use of ice-liquid water potential temperature as a thermodynamic variable in deep atmospheric models. Mon Weather Rev 1981;109:1094–102.
[12] Mellor GL, Yamada T. A hierarchy of turbulence closure models for planetary boundary layers. J Atmos Sci 1974;31:1791–806.
[13] Clark TL, Farley RD. Severe downslope windstorm calculations in two and three spatial dimensions using anelastic interactive grid nesting: a possible mechanism for gustiness. J Atmos Sci 1984;41:329–50.
[14] Louis JF. A parametric model of vertical eddy fluxes in the atmosphere. Bound Layer Meteorol 1979;17:187–202.
[15] Chen C, Cotton WR. The sensitivity of a simulated extratropical mesoscale convective system to long wave radiation and ice-phase microphysics. J Atmos Sci 1987;45:3897–910.
[16] Lee TJ. The impact of vegetation on the atmospheric boundary layer and convective storms. *Atmospheric Paper* No. 509. Fort Collins, CO: Dept. Atmos. Sci., Colorado State Univ; 1992.
[17] Tsuchiya M, Ishihara T, Fukumoto Y, Sukegawa H, Okubo K. The wind observation on Pacific ocean for the offshore wind farm. In: 19th Wind Engineering Symposium; 2006 [In Japanese].
[18] Suguro Y. History of large wind turbine in MHI and the development of 2400 kW wind turbine. J Jpn Wind Energy Assoc 2006;30(1):14–8 [in Japanese].
[19] IEC 61400-12. Wind turbine generator systems – part 12: wind turbine power performance testing; 1998.
[20] TEPCO illustrated. Tokyo Electric Power Company; 2010.

Further Reading

[1] Hayashi H, Uematsu T, Suzuki Y, Suzuki S, Sasaki R, Murakami S, et al. A new wind energy prediction model based on the CFD theory. In: Proc. World Wind Energy Conference (CD-ROM); 2002.
[2] Tanigawa R, Hayasaki N, Takagi T, Fukuda H, Shigaki D, Tsuyuki K. Wind resource assessment, based on "Wind turbine siting method and wind power prediction methods". In: Proc. 24th Symposium of Japan Wind Energy Association; 2002. pp. 119–22 [in Japanese].